FRACTURE, DELAMINATION, AND BUCKLING OF ELASTIC THIN FILMS ON COMPLIANT SUBSTRATES

Haixia Mei, Yaoyu Pang, Se Hyuk Im, Rui Huang
Department of Aerospace Engineering and Engineering Mechanics
University of Texas at Austin
1 University Station, C0600
Austin, Texas 78712
Phone: (512) 471-7558
Fax: (512) 471-5500
Email: ruihuang@mail.utexas.edu

ABSTRACT

A series of studies have been conducted for mechanical behavior of elastic thin films on compliant substrates. Under tension, the film may fracture by growing channel cracks. The driving force for channel cracking (i.e., the energy release rate) increases significantly for compliant substrates. Moreover, channel cracking may be accompanied by interfacial delamination. For a film on a relatively compliant substrate, a critical interface toughness is predicted, which separates stable and unstable delamination. For a film on a relatively stiff substrate, however, a channel crack grows with no delamination when the interface toughness is greater than a critical value. An effective energy release rate for the steady-state growth of a channel crack is defined to account for the influence of interfacial delamination on both the fracture driving force and the resistance, which can be significantly higher than the energy release rate assuming no delamination. Alternatively, when the film is under compression, it tends to buckle. Two buckling modes have been observed, one with interfacial delamination (i.e., buckle-delamination) and the other without delamination (i.e., wrinkling). By comparing the critical stresses for the onset of buckling, we give a criterion for the selection of the buckling modes, which depends on the stiffness ratio between the film and the substrate as well as the interface defects. A general conclusion from these studies is that, whether tension or compression, the interfacial properties are critical in controlling the morphology and failure of elastic thin films on compliant substrates.

KEY WORDS: fracture, delamination, buckling, interface

NOMENCLATURE

E	elastic modulus (N/m^2)
G	energy release rate (J/m^2)
K	stress intensity factor ($N\ m^{1/2}$)
W	fracture energy (J/m^2)
b	half width of buckle-delamination (m)
d	delamination width (m)
h	thickness (m)

Greek symbols

Γ	fracture toughness (J/m^2)
α	first Dundurs parameter (dimensionless)
β	second Dundurs parameter (dimensionless)
δ	opening displacement (m)
ψ	phase angle of mode mix (radian)
ν	Poisson's ratio (dimensionless)
σ	stress (N/m^2)

Subscripts

f	film
i	interface
s	substrate
ss	steady state

INTRODUCTION

Integrated structures with mechanically soft components have recently been pursued over a wide range of novel applications, from high performance integrated circuits in microelectronics [1] to unconventional organic electronics [2] and stretchable electronics [3,4], along with the ubiquitous integration of hard and soft materials in biomedical systems [5]. In particular, the integration of low dielectric constant (low k) materials in advanced interconnects of microelectronics has posed significant challenges for reliability issues due to compromised mechanical properties. Two common failure modes have been reported, one for cohesive fracture [6] and the other for interfacial delamination [7]. The former pertains to the brittleness of the low-k materials subjected to tension, and the latter manifests due to poor adhesion between low-k and surrounding materials. Furthermore, a thin film layer under compression can buckle, which leads to failure due to uneven surfaces, buckle-driven delamination and/or fracture [8,9]. These failure mechanisms are schematically illustrated in Figure 1. In this paper, the influence of interfacial delamination on fracture and buckling of elastic thin films is investigated, with an emphasis on applications with compliant substrates.

978-1-4244-1701-8/08/$25.00 ©2008 IEEE

CHANNEL CRACKING

One common cohesive fracture mode for thin films under tension is channel cracking (Figure 1a). Previous studies have shown that the driving force (i.e., the energy release rate) for the steady-state growth of a channel crack depends on the constraint effect of surrounding layers [10-12]. For a brittle thin film on an elastic substrate, the driving force increases for increasingly compliant substrates. The effect of constraint can be partly lost as the substrate deforms plastically [13] or viscoelastically [14,15]. More recent studies have investigated the effects of stacked buffer layers [16,17] and patterned film structures [6]. In most of these studies, the interfaces between the film and the substrate or the buffer layers are assumed to remain perfectly bonded as the channel crack grows in the film (Figure 1a). Under this assumption, the energy release rate for the steady-state growth of a channel crack in a thin elastic film bonded to a thick elastic substrate is:

$$G_{ss} = Z(\alpha,\beta)\frac{\sigma_f^2 h_f}{\bar{E}_f}, \quad (1)$$

where σ_f is the tensile stress in the film, h_f is the film thickness, and $\bar{E}_f = E_f/(1-\nu_f^2)$ is the plane strain modulus of the film with Young's modulus E_f and Poisson's ratio ν_f. The dimensionless coefficient Z depends on the elastic mismatch between the film and the substrate, through the Dundurs' parameters

$$\alpha = \frac{\bar{E}_f - \bar{E}_s}{\bar{E}_f + \bar{E}_s}, \quad (2)$$

$$\beta = \frac{\bar{E}_f(1-\nu_f)(1-2\nu_s) - \bar{E}_s(1-\nu_s)(1-2\nu_f)}{2(1-\nu_f)(1-\nu_s)(\bar{E}_f + \bar{E}_s)}. \quad (3)$$

When the film and the substrate have identical elastic moduli, we have $\alpha = \beta = 0$ and $Z = 1.976$. The value of Z decreases slightly for a compliant film on a relatively stiff substrate ($\bar{E}_f < \bar{E}_s$ and $\alpha < 0$). A more compliant substrate ($\alpha > 0$), on the other hand, provides less constraint against film cracking. Thus, Z increases as α increases. For very compliant substrates (e.g., low-k dielectrics, polymers, etc.), Z increases rapidly, with $Z > 30$ for $\alpha > 0.99$ [11,12]. The effect of β is secondary and often ignored.

In general, the steady-state energy release rate of channel cracking can be calculated from a two-dimensional (2D) model [10-12] as follows:

$$G_{ss} = \frac{1}{2h_f}\int_0^{h_f} \sigma_f \delta(z)dz, \quad (4)$$

where $\delta(z)$ is the opening displacement of the crack surfaces far behind the channel front. Due to the constraint by the substrate, the crack opening does not change as the channel front advances and the energy release rate attains a steady state, independent of the channel length. Three-dimensional analyses have shown that the steady state is reached when the length of a channel crack exceeds two to three times the film thickness for a relatively stiff substrate [18], but the crack length to reach the steady state can be significantly longer for more compliant substrate materials [13]. The present study focuses on the steady state.

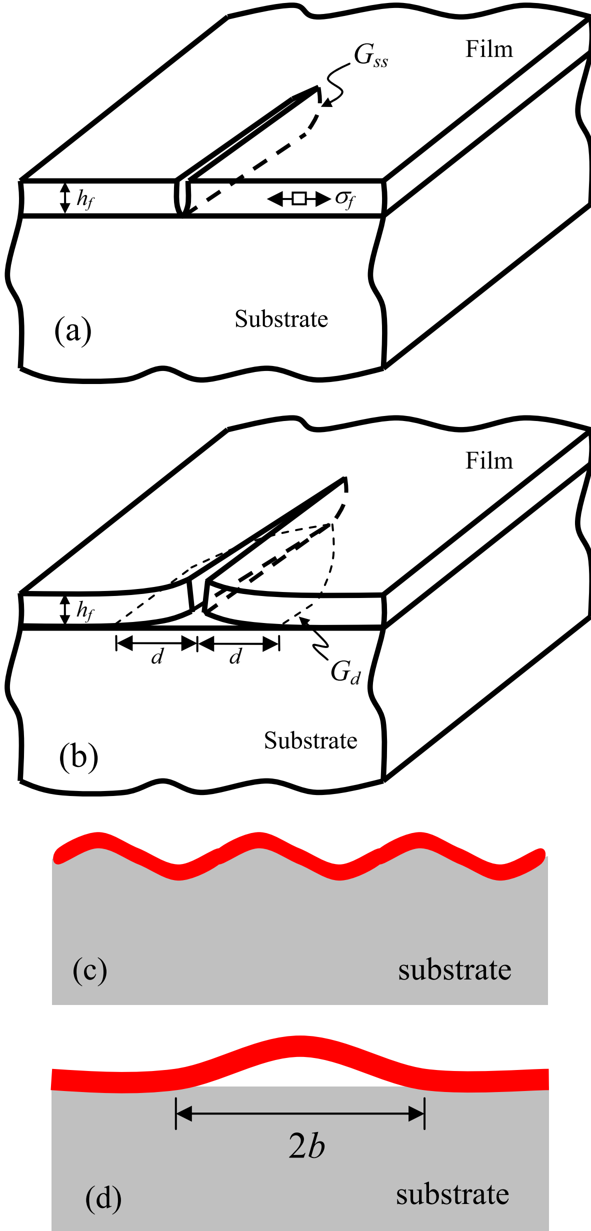

Fig. 1: Schematic illustration of common failure mechanisms in thin film structures: (a) channel cracking; (b) concomitant channel cracking and interfacial delamination; (c) wrinkling; (d) buckle-delamination.

INTERFACIAL DELAMINATION FROM CHANNEL

While some experimental observations clearly showed channel cracks with no delamination [16,19], others observed delamination of the interface [16,20]. There are two questions to be answered: *First, under what condition would the growth*

of a channel crack be accompanied by interfacial delamination? Second, how would the interfacial delamination (if occurring) affect the fracture condition or reliability in integrated thin film structures? To answer these questions, we consider in this section interfacial delamination emanating from the root of a channel crack (Fig. 1b). For a long, straight channel crack, we assume a steady state far behind the channel front, where the interfacial crack has a finite width, *d*. The energy release rate for the interfacial crack can be written in a similar form as Eq. (1):

$$G_d = Z_d\left(\frac{d}{h_f},\alpha,\beta\right)\frac{\sigma_f^2 h_f}{\bar{E}_f}, \tag{5}$$

where Z_d is a dimensionless function that can be determined from a two-dimensional plane strain problem [21]. In the present study, a finite element model is constructed to calculate the interfacial energy release rate. The finite element package ABAQUS is employed. The method of J-integral is adopted for the calculation of the interfacial energy release rate. In all calculations, we set $\nu_f = \nu_s = 1/3$ such that $\beta = \alpha/4$, while the mismatch parameter α is varied.

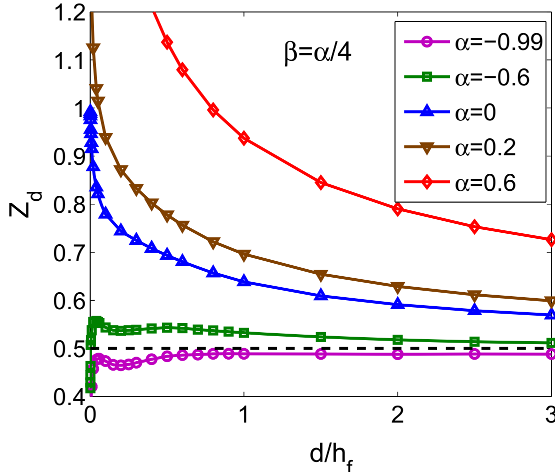

Fig. 2: Normalized energy release rate of interfacial delamination from the root of a channel crack as a function of the normalized delamination width for different elastic mismatch parameters.

As shown in Figure 2, the Z_d function has two limits. First, when $d/h_f \to \infty$ (long crack limit), the interfacial crack reaches a steady state with the energy release rate

$$G_{ss}^d = \frac{\sigma_f^2 h_f}{2\bar{E}_f}, \tag{6}$$

and thus $Z_d \to 0.5$. The steady-state energy release rate for the interfacial crack is independent of the elastic mismatch. On the other hand, when $d/h_f \to 0$ (short crack limit), the interfacial energy release rate follows a power law [22]:

$$Z_d \sim \left(\frac{d}{h_f}\right)^{1-2\lambda}, \tag{7}$$

where λ depends on the elastic mismatch and can be determined by solving the equation [23]

$$\cos\lambda\pi = \frac{2(\beta-\alpha)}{1+\beta}(1-\lambda)^2 + \frac{\alpha+\beta^2}{1-\beta^2}. \tag{8}$$

Here we discuss three scenarios at the short crack limit, which would eventually determine the condition for channel cracking with or without interfacial delamination. First, when $\alpha = \beta = 0$ (no elastic mismatch), we have $\lambda = 0.5$. In this case, Z_d approaches a constant as $d/h_f \to 0$. An analytical solution [21] predicts that $Z_d(0,0,0) \to 0.9878$, which compares closely with the numerical results (Fig. 2). When $\alpha > 0$, we have $\lambda > 0.5$. Consequently, $Z_d \to \infty$ as $d/h_f \to 0$. As shown in Figure 2, for both $\alpha = 0$ and $\alpha > 0$, the interfacial energy release rate monotonically decreases as the delamination width increases. On the other hand, when $\alpha < 0$, we have $0 < \lambda < 0.5$, and thus, $Z_d \to 0$ as $d/h_f \to 0$. Interestingly, the numerical results in Figure 2 show that, instead of a monotonic variation with respect to the crack length, the interfacial energy release rate oscillates between the short and long crack limits for the cases with $\alpha < 0$. Such an oscillation leads to local maxima of the interfacial energy release rate, which in some cases (e.g., $\alpha = -0.6$) can be greater than the steady state value at the long crack limit.

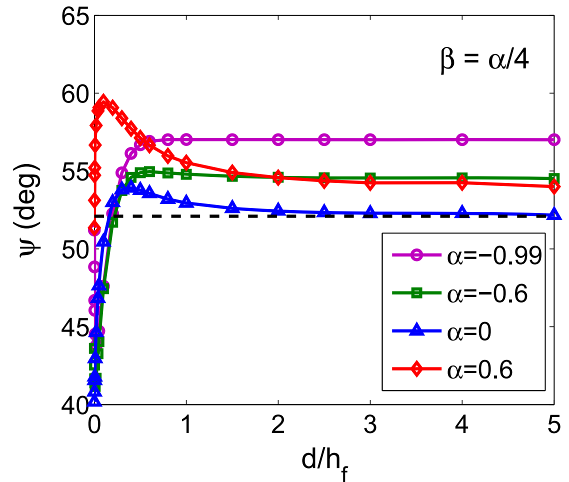

Fig. 3: Phase angle of the mode mix for interfacial delamination as a function of the normalized delamination width for different elastic mismatch parameters. The dashed line indicates of the steady-state phase angle (52°) for the case of zero elastic mismatch ($\alpha = \beta = 0$).

A necessary condition for steady-state channel cracking with concomitant interfacial delamination is that the interfacial crack arrests at a finite width. The delamination width can thus be determined by comparing the interfacial energy release rate in Eq. (5) to the interface toughness. In general, the interface toughness depends on the phase angel of mode mix [10], which in turn depends on the delamination width, as shown in Figure 3. Due to the oscillatory nature of the stress singularity at the interfacial crack tip [24], a length scale has to be used to

define the phase angle. Here we take the film thickness h_f as the length scale, and define the mode angle as

$$\psi = \tan^{-1}\left(\frac{\mathrm{Im}\left(Kh_f^{i\varepsilon}\right)}{\mathrm{Re}\left(Kh_f^{i\varepsilon}\right)}\right), \tag{9}$$

where $K = K_1 + iK_2$ is the complex stress intensity factor, and $\varepsilon = \frac{1}{2\pi}\ln\left(\frac{1-\beta}{1+\beta}\right)$. The real and imaginary parts of the complex stress intensity factor are calculated by the interaction integral method in ABAQUS. Figure 3 shows that the phase angle quickly approaches a steady state, $\psi_{ss} = \omega(\alpha,\beta)$. When the film and the substrate have identical elastic moduli ($\alpha = \beta = 0$), we have $\psi_{ss} = \omega(0,0) = 52^\circ$. Considering the fact that the variation of the phase angle with respect to the delamination width is relatively small and confined within a small range of short cracks ($d < h_f$), we take the constant steady-state phase angle in the subsequent discussions and assume that the interface toughness is independent of the delamination width, i.e., $\Gamma_i = \Gamma_i(\psi_{ss})$. Then, the width of the interfacial delamination can be determined by requiring that

$$Z_d\left(\frac{d_s}{h_f},\alpha,\beta\right) = \bar{\Gamma}_i = \frac{\bar{E}_f\Gamma_i(\psi_{ss})}{\sigma_f^2 h_f}. \tag{10}$$

Depending on the elastic mismatch parameters and the normalized interface toughness ($\bar{\Gamma}_i$), the solution to Eq. (10) predicts no delamination ($d_s = 0$), stable finite delamination ($0 < d_s < \infty$), or unstable delamination ($d_s \to \infty$). The result is summarized in Figure 4 as an interfacial delamination map. In particular, for a stiff film on a relatively compliant substrate ($\alpha > 0$), a stable delamination along the channel crack is predicted for $\bar{\Gamma}_i > 0.5$, whereas unstable delamination is predicted for $\bar{\Gamma}_i \le 0.5$. On the other hand, on a relatively stiff substrate ($\alpha < 0$), the film cracks with no delamination in Region I. The boundary between Region I and Region II-B is determined from the finite element calculations, corresponding the maximum interfacial energy release rate in the range $0 > \alpha > -0.89$ (see Fig. 2 for $\alpha = -0.6$).

In an experimental study by Tsui et al. [16], no interfacial delamination was observed for channel cracking of a low k film directly deposited on a Si substrate, while a finite delamination was observed when a polymer buffer layer was sandwiched between the film and the substrate. These observations are consistent with the delamination map. In the former case, the elastic mismatch between the film and the substrate, $\alpha = -0.91$, thus no delamination when the normalized interface toughness $\bar{\Gamma}_i \ge 0.5$ (i.e., Region I in Fig. 4). With a polymer buffer layer, however, the elastic mismatch between the low k material and the polymer is, $\alpha = 0.4$. Although the polymer layer is relatively thin, it qualitatively changes the interfacial behavior from that for $\alpha < 0$ (Region I) to that for $\alpha > 0$ (Region II-A). More experimental evidences with different combinations of elastic mismatch, interface toughness, and film stress would be needed for further validation of the predicted delamination map.

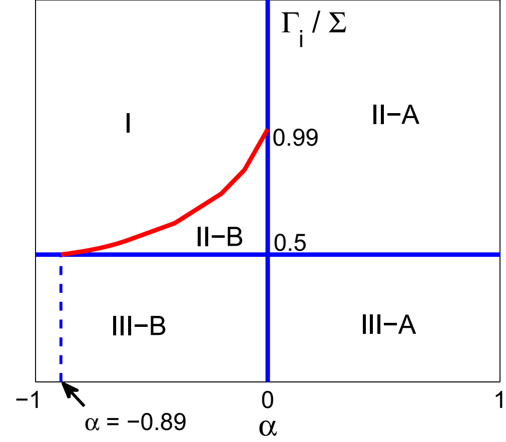

Fig. 4. A map for interfacial delamination from the root of a channel crack: (I) no delamination, (II) stable delamination, and (III) unstable delamination, where A and B denote delamination without and with an initiation barrier, respectively.

CONCOMITANT CRACKING AND DELAMINATION

With a stable delamination along each side of the channel crack (Fig. 1b), the substrate constraint on the opening of the channel crack is relaxed. Consequently, the steady-state energy release rate calculated from Eq. (4) becomes greater than Eq. (1). A dimensional consideration leads to

$$G_{ss}^* = Z^*\left(\frac{d_s}{h_f},\alpha,\beta\right)\frac{\sigma_f^2 h_f}{\bar{E}_f}, \tag{11}$$

where Z^* is a new dimensionless coefficient that depends on the width of interfacial delamination (d_s/h_f) in addition to the elastic mismatch parameters.

The same finite element model is employed to calculate G_{ss}^*, by integrating the opening displacement along the surface of the channel crack as in Eq. (3). The stable delamination width, d_s/h_f, is obtained as a function of the normalized interface toughness, $\bar{\Gamma}_i$, by Eq. (10). Thus, the coefficient Z^* is plotted as a function of $\bar{\Gamma}_i$, as shown in Figure 5. When $\alpha > 0$, $Z^* \to Z$ as $\bar{\Gamma}_i \to \infty$, and $Z^* \to \infty$ as $\bar{\Gamma}_i \to 0.5$; in between, Z^* increases as $\bar{\Gamma}_i$ decreases, because the interfacial delamination width increases. When $\alpha = 0$, $Z^* = Z$ for $\bar{\Gamma}_i \ge 0.9878$ (i.e., no delamination). When $0 > \alpha > -0.89$, Z^* increases from Z to infinity within a narrow window of $\bar{\Gamma}_i$, where stable delamination is predicted (Region II-B in Fig. 4). For $\alpha < -0.89$, either $Z^* = Z$ for no delamination or $Z^* \to \infty$ for unstable delamination. Apparently, with interfacial delamination, the driving force for channel cracking can be significantly higher than that assuming no delamination.

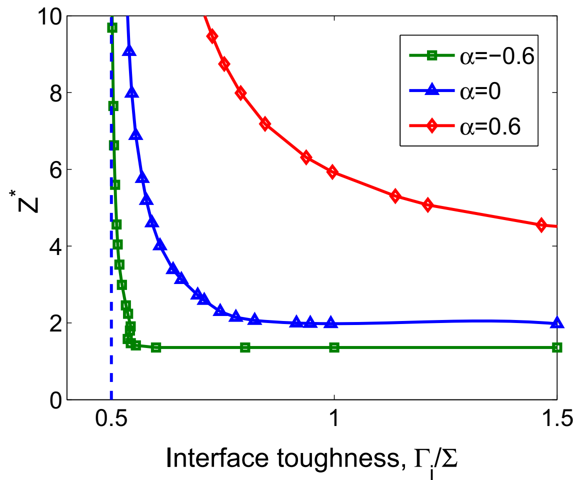

Fig. 5. Influence of the normalized interface toughness ($\Sigma = \sigma_f^2 h_f / \overline{E}_f$) on the steady-state driving force for channel cracking.

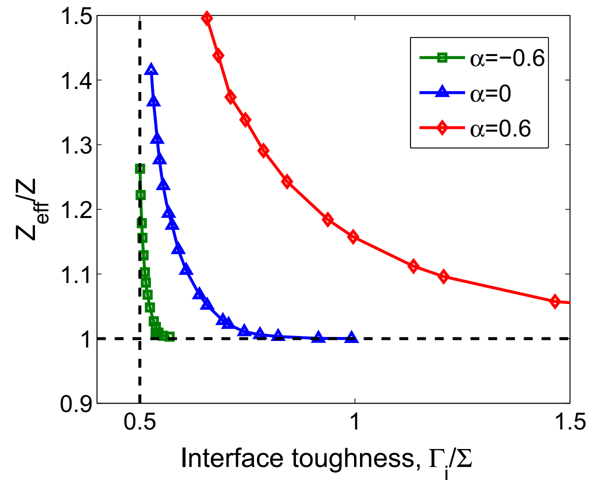

Fig. 6. Effective driving force for steady-state channel cracking as a function of the normalized interface toughness ($\Sigma = \sigma_f^2 h_f / \overline{E}_f$).

While the interfacial delamination, if occurring, relaxes the constraint on crack opening thus enhances the fracture driving force, it also requires additional energy to fracture the interface as the channel crack advances. An energetic condition can thus be stated: if the increase in the energy release exceeds the fracture energy needed for delamination, growth of the channel crack with interfacial delamination is energetically favored; otherwise, the channel crack grows with no delamination. Considering the interfacial fracture energy, a modified fracture condition for steady-state growth of a channel crack can be written as

$$G_{ss}^* \geq \Gamma_f + W_d, \tag{12}$$

where Γ_f is the cohesive fracture toughness of the film, and W_d is the energy required to delaminate the interface accompanying per unit area growth of the channel crack. For stable delamination of width $d = d_s$ at both sides of a channel crack, the delamination energy is

$$W_d = \frac{2}{h_f} \int_0^{d_s} \Gamma_i(\psi(a)) da \approx 2\Gamma_i(\psi_{ss}) \frac{d_s}{h_f}. \tag{13}$$

Equation (12) may not be convenient to apply directly, since both sides of the equation (driving force and resistance, respectively) increase with the interfacial delamination. By moving W_d to the left hand side and noting that the stable delamination width is a function of the interface toughness, we define an effective driving force for the steady-state channel cracking

$$G_{ss}^{eff} = G_{ss}^* - W_d = Z_{eff}(\overline{\Gamma}_i, \alpha, \beta) \frac{\sigma_f^2 h_f}{\overline{E}_f}, \tag{14}$$

with

$$Z_{eff} = Z^*\left(\frac{d_s}{h_f}, \alpha, \beta\right) - 2\overline{\Gamma}_i \frac{d_s}{h_f}. \tag{15}$$

Using the effective energy release rate, the condition for the steady-state channel cracking is simply a comparison between G_{ss}^{eff} and Γ_f, the latter being a constant independent of the interface. Figure 6 plots the ratio, $Z_{eff}/Z(\alpha,\beta)$, as a function of $\overline{\Gamma}_i$ for different elastic mismatch parameters. At the limit of high interface toughness ($\overline{\Gamma}_i \to \infty$), $d_s \to 0$ and $Z_{eff} \to Z$, which recovers the case of channel cracking with no delamination. The effective driving force increases as the normalized interface toughness deceases.

The present study predicts that channel cracking in an elastic thin film on a relatively compliant substrate is always accompanied by interfacial delamination, either stable or unstable, depending on the interface toughness. This differs from the case for an elastic film on a relatively stiff substrate, in which channel cracks may grow without interfacial delamination (Region I in Fig. 4). This difference may have important implications for reliability of integrated structures. As an example, for interconnect structures in microelectronics, the low-k dielectrics is usually more compliant compared to the surrounding materials [6]. Therefore, fracture of the low-k dielectrics by channel cracking is typically not accompanied by interfacial delamination. However, when a more complaint buffer layer is added adjacent to the low-k film, interfacial delamination can occur concomitantly with channel cracking of the low-k film [16]. Moreover, a relatively stiff cap layer (e.g., SiN) is often deposited on top of the low-k film [7]. Channel cracking of the cap layer on low-k could be significantly enhanced by interfacial delamination. Flexible electronics is another area of applications where compliant substrates have to be used extensively along with mechanically stiffer films for the functional devices and interconnects [3,4]. Here, interfacial delamination could play a critical role in the reliability assessment. As shown in a previous study [25], the stretchability of metal thin-film interconnects on a compliant substrate can be dramatically reduced by interfacial delamination. For brittle thin films on compliant substrates, as considered in the present study,

interfacial delamination has a similar effect on the fracture and thus deformability of the devices.

WRINKLING AND BUCKLE-DELAMINATION

Upon compression, buckling of thin films may lead to failure of integrated structures interfacial delamination and fracture [8,9]. Recently, understanding of buckle patterns has also led to applications in metrology [26,27], stretchable interconnects [28,29], and optical gratings [30]. Previous studies on thin film buckling have focused on one of the two buckling modes, *buckle-delamination* or *wrinkling*, as illustrated in Fig. 1(c) and (d). The former considers buckling of the film when it is partly delaminated from the substrate [10], while the latter assumes no delamination as the substrate deforms coherently with the film [31]. The characteristics of both buckling modes are often observable, with localized patterns for buckle-delamination (e.g., telephone cord blisters) and homogeneous patterns for wrinkling. One of the unanswered questions is: *what determines the selection of either buckling mode for a given material system?*

For a thin elastic film bonded to a thick elastic substrate, the buckling instability is constrained by the substrate. Without delamination, buckling of the film (i.e., wrinkling) requires coherent deformation of the substrate, which is possible only when the substrate is relatively compliant. Based on an energetic analysis [31], the critical stress for wrinkling is

$$\sigma_w = \frac{\bar{E}_f}{4}\left(\frac{3\bar{E}_s}{\bar{E}_f}\right)^{2/3}. \tag{16}$$

When the compressive stress in the film, $\sigma_f > \sigma_w$, the film buckles spontaneously, forming wrinkles throughout the film surface. A particular wrinkle wavelength is established to minimize the total elastic energy in the film and the substrate [31]. The effects of substrate and film thicknesses on the wrinkling stress have also been studied previously [31,32].

For stiff substrates, buckling deformation of the film is highly constrained, leading to high critical stresses for wrinkling. However, the substrate constraint may be locally mitigated by interfacial defects that lead to partial delamination of the film. In this case, the delaminated portion of the film buckles, which in turn drives growth of delamination through interfacial fracture [10]. The co-development of buckling and delamination leads to abundant blister patterns such as telephone-cord blisters. Compared to wrinkling, the buckle-delamination patterns are typically localized and sensitive to interfacial defects [33,34]. Early studies of buckle-delamination often assumed a fixed-end condition at the edge of delamination, which essentially neglected the effect of elastic deformation in the substrate. Under such a condition, the critical stress for the onset of buckling is

$$\sigma_{B0} = \frac{\pi^2}{12}\left(\frac{h_f}{b}\right)^2 \bar{E}_f, \tag{17}$$

where b is the half width of the delamination (Fig. 1d). The buckling stress σ_{B0} is independent of the substrate properties but depends on the relative size of the interfacial delamination.

Recent studies [35-37] have shown that the buckling stress can be significantly lower than that predicted by Eq. (17) when the elastic deformation of the substrate is considered, especially for compliant substrates. Yu and Hutchinson [37] derived an implicit expression for the critical stress:

$$\sqrt{\frac{\sigma_{B0}}{\sigma_B}}\tan\left(\pi\sqrt{\frac{\sigma_B}{\sigma_{B0}}}\right) = \frac{\pi h_f}{12b}\left(\frac{a_{12}^2}{b/h_f + a_{11}} - a_{22}\right), \tag{18}$$

where a_{11}, a_{22}, and a_{12} are determined numerically, either by direct finite element calculations or by solving an integral equation, as dimensionless spring constants at the edge of the buckled film, which depend on the ratio b/h_f and the Dundurs' parameters.

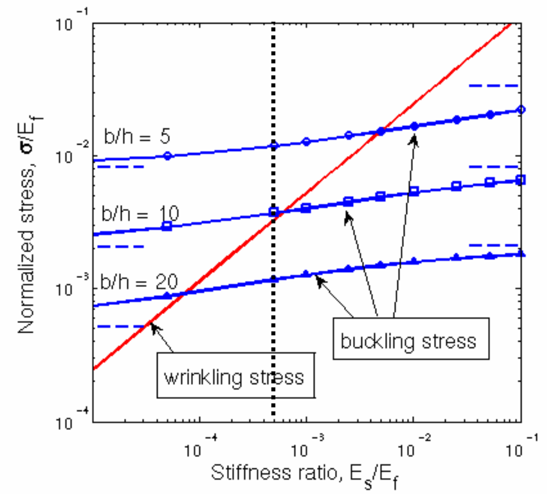

Fig. 7: Comparison between the critical stresses for wrinkling and buckle-delamination. The open symbols are numerical results from Eq. (18). The dashed lines indicate the limiting stresses for buckle-delamination. The vertical line represents the PS/PDMS system with $\bar{E}_s/\bar{E}_f = 0.0005$.

A comparison between the critical stresses for wrinkling and buckle-delamination is presented in Fig. 7. The stresses are normalized by the plane-strain modulus of the film and plotted versus the substrate-film stiffness ratio. Using the log-log scales, the critical wrinkling stress in Eq. (16) is a straight line with a slope 2/3. The critical stress for buckling, σ_B, obtained from Eq. (3), decreases as the relative delamination size b/h increases. For a constant delamination size, the buckling stress increases as the stiffness ratio increases, but at a slower rate compared to the increase of the wrinkling stress. The intersection of the two critical stresses defines a critical stiffness ratio, R_c. When the relative substrate stiffness is greater (i.e., $\bar{E}_s/\bar{E}_f > R_c$), the buckling stress is lower than the wrinkling stress, dictating that buckle-delamination occurs first as the compressive stress develops in the film. On the other hand, for more compliant substrates ($\bar{E}_s/\bar{E}_f < R_c$), the wrinkling stress is lower and the film wrinkles. Therefore, a transition in the buckling mode is predicted quantitatively as

the stiffness ratio between the substrate and the film varies. The critical value R_c as a function of the delamination size is plotted in Fig. 8. This plot represents a *buckling mode selection map*: if the stiffness ratio and the interfacial defect size render a point below the R_c curve, wrinkling is energetically favored; otherwise, buckle-delamination is favored.

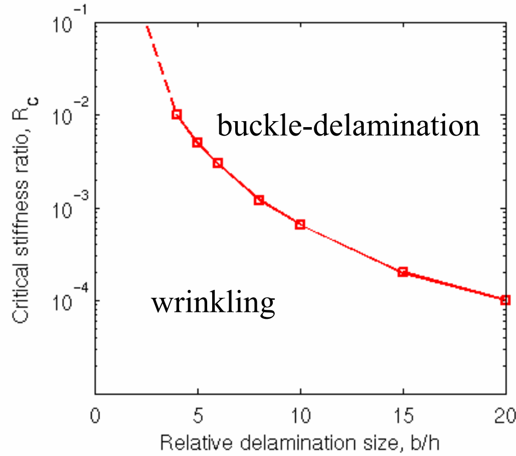

Fig. 8: The critical stiffness ratio as a function of the relative delamination size.

To validate the buckling mode selection criterion described above, an experiment was conducted, which observed both buckling modes as well as a mode transition [38]. A polystyrene (PS) film (h_f = 120 nm) was bonded to a 1 mm thick polydimethylsiloxane (PDMS) substrate. The materials' elastic moduli are estimated as $\overline{E}_f \sim 4$ GPa and $\overline{E}_s \sim 2$ MPa, with a ratio $\overline{E}_s / \overline{E}_f = 0.0005$. By annealing the specimen at 120 °C, which is above the glass transition temperature of PS ($T_g \sim 105$ ºC), and then slowly cooling, a compressive stress develops in the PS film due to differential thermal expansion. Assuming an initially small defect at the interface (say, $b/h_f = 5$), as illustrated by the vertical line in Fig. 7, the compressive stress in the PS film first reaches the wrinkling stress, at which point wrinkling occurs spontaneously over the film surface. As the temperature is further decreased, the stress eventually reaches the critical buckling stress for the initial defect size, and buckle-delamination occurs alongside the existing wrinkles. When the material system was heated back to 120 °C from the room temperature, the compressive stress in the film vanished and the elastic film recovered with no observable buckling or wrinkling. Next, the system was subjected to a second cooling. Compared to the first cooling, the interfacial defect size has increased due to the growth of buckle-delamination in the first cycle. An estimate of the delamination width gives $b/h_f \sim 20$ for the second cycle, for which the buckling stress is lower than the wrinkling stress as shown in Fig. 7. Consequently, buckle-delamination occurred first. Further cooling led to growth of buckle-delamination and eventually wrinkling of the bonded region as well.

SUMMARY

This paper considers fracture and buckling of elastic thin films under the influence of interfacial delamination. Three main conclusions are summarized as follows.

- Stable interfacial delamination along a channel crack is predicted for certain combinations of film/substrate elastic mismatch, interface toughness, and film stress, as summarized in a delamination map (Fig. 4), together with conditions for no delamination and unstable delamination.
- Interfacial delamination not only increases the fracture driving force for steady-state growth of the channel crack, but also adds to the fracture resistance by requiring additional energy for the interfacial fracture. An effective energy release rate for channel cracking is defined, which depends on the interface toughness (Fig. 6) in addition to the elastic mismatch and can be considerably higher than the energy release rate assuming no delamination.
- Under compression, the film may buckle with or without delamination. The onset of the buckling and the selection of the buckling mode depend on the elastic mismatch and the pre-existing interfacial defects, as summarized in a buckling map (Fig. 8).

Acknowledgments

The authors are grateful for the financial support by National Science Foundation under Grant No. 0547409.

References

[1] P. S. Ho, G. Wang, M. Ding, J. H. Zhao, X. Dai, "Reliability issues for flip-chip packages," Microelectronics Reliability, vol. 44, pp. 719-737, 2004.

[2] A. Dodabalapur, "Organic and polymer transistors for electronics," Materials Today, vol. 9, pp. 24-30, 2006.

[3] S. Wagner, S. P. Lacour, J. Jones, P. I. Hsu, J. C. Sturm, T. Li, Z. Suo, "Electronic skin: architecture and components," Physica E, vol. 25, pp. 326-334, 2004.

[4] D. Y. Khang, H. Q. Jiang, Y. Huang, J. A. Rogers, "A stretchable form of single-crystal silicon for high-performance electronics on rubber substrate," Science, vol. 311, pp. 208-212, 2006.

[5] H. Gao, "Application of fracture mechanics concepts to hierarchical biomechanics of bone and bone-like materials," Int. J. Fracture 138: 101–137, 2006.

[6] X. H. Liu, M. W. Lane, T. M. Shaw, E. G. Liniger, R. R. Rosenberg, D. C. Edelstein, "Low-k BEOL mechanical modeling," Proc. Advanced Metallization Conference, pp. 361-367, 2004.

[7] X. H. Liu, M. W. Lane, T. M. Shaw, E. Simonyi, "Delamination in patterned films," Int. J. Solids Struct., vol 44, pp. 1706-1718, 2007.

[8] J. W. Hutchinson, M. D. Thouless, E. G. Liniger, "Growth and configurational stability of circular, buckling-driven film

delaminations," Acta Metall. Mater., vol. 40, pp. 295-308, 1992.

[9] H. Yin, R. Huang, K. D. Hobart, J. Liang, Z. Suo, S. R. Shieh, T. S. Duffy, F. J. Kub, J. C. Sturm, "Buckling suppression of SiGe islands on compliant substrates," J. Appl. Phys., vol. 94, pp. 6875-6882, 2003.

[10] J. W. Hutchinson, Z. Suo, "Mixed mode cracking in layered materials," Advances in Applied Mechanics, vol. 29, pp. 63-191, 1992.

[11] J. L. Beuth, "Cracking of thin bonded film in residual tension," Int. J. Solids Struct., vol. 29, pp. 1657-1675, 1992.

[12] R. Huang, J. H. Prevost, Z. Y. Huang, Z. Suo, "Channel-cracking of thin films with the extended finite element method," Eng. Frac. Mech., vol. 70, pp. 2513-2526, 2003.

[13] J. M. Ambrico, M. R. Begley, "The role of initial flaw size, elastic compliance and plasticity in channel cracking of thin films," Thin Solid Films, vol. 419, pp. 144-153, 2002.

[14] R. Huang, J. H. Prevost, Z. Suo, "Loss of constraint on fracture in thin film structures due to creep," Acta Mater., vol. 50, pp. 4137-4148, 2002.

[15] Z. Suo, J. H. Prevost, J. Liang, "Kinetics of crack initiation and growth in organic-containing integrated structures," J. Mech. Phys. Solids, vol. 51, pp. 2169-2190, 2003.

[16] T. Y. Tsui, A. J. McKerrow, J. J. Vlassak, "Constraint effects on thin film channel cracking behavior," J. Mater. Res., vol. 20, pp. 2266-2273, 2005.

[17] N. Cordero, J. Yoon, Z. Suo, "Channel cracks in hermetic coating consisting of organic and inorganic layers," Appl. Phys. Lett., vol. 90, 111910, 2007.

[18] T. Nakamura, S. M. Kamath, "Three-dimensional effects in thin-film fracture mechanics," Mech. Mater., vol. 13, pp. 67-77, 1992.

[19] J. He, G. Xu, Z. Suo, "Experimental determination of crack driving forces in integrated structures," Proc. 7th Int. Workshop on Stress-Induced Phenomena in Metallization (Austin, Texas, 14-16 June 2004), pp. 3-14, 2004.

[20] Z. Suo, "Reliability of Interconnect Structures," In Volume 8: Interfacial and Nanoscale Failure (W. Gerberich, W. Yang, Editors) of *Comprehensive Structural Integrity* (I. Milne, R.O. Ritchie, B. Karihaloo, Editors-in-Chief), Elsevier, Amsterdam, pp. 265-324, 2003.

[21] H. Mei, Y. Pang, R. Huang, "Influence of interfacial delamination on channel cracking of elastic thin films," Int. J. Fracture, submitted, December 2007.

[22] M. Y. He, J. W. Hutchinson, "Crack deflection at an interface between dissimilar elastic materials," Int. J. Solids Struct., vol. 25, pp. 1053-1067, 1989.

[23] A. R. Zak, M. L. Williams, "Crack point stress singularities at a bi-material interface," J. Appl. Mech., vol. 30, pp. 142-143, 1963.

[24] J. R. Rice, "Elastic fracture concepts for interfacial cracks," J. Appl. Mech., vol. 55, pp. 98-103, 1988.

[25] T. Li, Z. Suo, "Ductility of thin metal films on polymer substrates modulated by interfacial adhesion," Int. J. Solids Struct., vol. 44, pp. 1696-1705, 2007.

[26] C. M. Stafford, C. Harrison, K. L. Beers, A. Karim, E. J. Amis, M. R. VanLandingham, H.-C. Kim, W. Volksen, R. D. Miller, E. E. Simonyi, "A buckling-based metrology for measuring the elastic moduli of polymeric thin films," Nat. Mater., vol. 3, pp. 545-550, 2004.

[27] C. M. Stafford, B. D. Vogt, C. Harrison, D. Julthongpiput, R. Huang, "Elastic moduli of ultrathin amorphous polymer films," Macromolecules, vol. 39, pp. 5095-5099, 2006.

[28] M. Watanabe, H. Shirai, T. Hirai, "Wrinkled polypyrrole electrode for electroactive polymer actuators," J. Appl. Phys., vol. 92, pp. 4631-4637, 2002.

[29] S. P. Lacour, S. Wagner, Z. Y. Huang, Z. Suo, "Stretchable gold conductors on elastomeric substrates," Appl. Phys. Lett., vol. 82, pp. 2404-2406, 2003.

[30] C. Harrison, C. M. Stafford, W. Zhang, A. Karim, "Sinusoidal phase grating created by a tunably buckled surface," Appl. Phys. Lett., vol. 85, pp. 4016-4018, 2004.

[31] R. Huang, "Kinetic wrinkling of an elastic film on a viscoelastic substrate," J. Mech. Phys. Solids, vol. 53, pp. 63-89, 2005.

[32] R. Huang, C. M. Stafford, B. D. Vogt "Effect of surface properties on wrinkling of ultrathin films," J. Aerospace Engineering, vol. 20, pp. 38-44, 2007.

[33] M.-W. Moon, J.-W. Chung, K.-R. Lee, K. H. Oh, R. Wang, A. G. Evans, "An experimental study of the influence of imperfections on the buckling of compressed thin films," Acta Mater., vol. 50, pp. 1219-1227, 2002.

[34] C. Coupeau, "Atomic force microscopy study of the morphological shape of thin film buckling," Thin Solid Films, vol. 406, pp. 190-194, 2002.

[35] B. Cotterell, Z. Chen, "Buckling and cracking of thin films on compliant substrate under compression," Int. J. Fracture, vol. 104, pp. 169-179, 2000.

[36] G. Parry, J. Colin, C. Coupeau, F. Foucher, A. Cimetiere, J. Grilhe, "Effect of substrate compliance on the global unilateral post-buckling of coatings: AFM observations and finite element calculations," Acta Mater., vol. 53, pp. 441-447, 2005.

[37] H. H. Yu, J.W. Hutchinson, "The influence of substrate compliance on thin film buckling delaminaton," Int. J. Fracture, vol. 113, pp. 39-55, 2001.

[38] H. Mei, J. Y. Chung, H.-H. Yu, C. M. Stafford, and R. Huang, "Buckling modes of elastic thin films on elastic substrates," Appl. Phys. Lett., vol. 90, 151902, 2007.